Proper Orthogonal Decomposition Analysis of a Turbulent Swirling Self-Excited Premixed Flame

A.M. Kypraiou [1], A.P. Dowling [2] and E. Mastorakos [3]
Department of Engineering, University of Cambridge, Cambridge CB2 1PZ, UK

and

N. Karimi [4]
School of Engineering, University of Glasgow, Glasgow G12 8QQ, UK

Thermoacoustic oscillations constitute a serious threat to the integrity of combustion systems. The goal of the present work is to determine the effect of the equivalence ratio (φ), inlet flow velocity (U), and burner geometry on the characteristics of the self-excited oscillations and to reveal the dominant mechanisms. It also focuses on the data post-processing aiming at extracting information about the dynamics that are not captured through classical ensemble-averaging, and hence the Proper Orthogonal Decomposition technique is used. Experiments were conducted with a fully-premixed air/methane flame stabilized on a conical bluff body. Self-excited acoustic instabilities were induced by extending the length of the combustion chamber downstream of the bluff body. The flame was visualised using OH* chemiluminescence and OH PLIF at 5 kHz. Proper Orthogonal Decomposition (POD) and Fast Fourier Transform analysis were conducted on the imaging data. A strong effect of the chamber length was found, which primarily drove the generation of acoustic oscillation and flame-vortex interaction. Significant differences in the flame roll-up were found when either the burner geometry or the equivalence ratio was altered. Changes were detected in the frequency of oscillations, which showed a general trend to increase with φ and U and decrease with the length of the duct. Analysis of the POD modes allowed an estimate of the convection speed of the flame structures associated with the dominant frequency and it was found that this convection speed was about 1.5 U for most conditions studied.

I. Introduction

COMBUSTION instability phenomena have for long been the centre of attention for several research groups. In a combustion system, heat release and acoustics interact, forming a closed loop, generating pressure oscillations through feedback coupling. A thorough understanding of the underlying mechanisms of instabilities is important to obtain because the pressure fluctuations subject the surfaces of the combustion chamber to increased heat loads, ultimately leading to performance degradation and system failure[1]. However, due to their complex nature, these mechanisms are far from being completely understood. Extraction of information about the fluctuating heat release rate has been greatly facilitated with the introduction of advanced imaging techniques in experiments. To date, several studies focusing on flow-flame dynamics have been conducted using either chemiluminescence or laser-induced fluorescence techniques on both self-excited and acoustically-excited flames[2-6]. Chemiluminescence emission measurements have been used to identify fluctuations in heat release rate, nevertheless they are characterised by poor spatial resolution since chemiluminescence is a line of sight technique. Planar laser-induced fluorescence (PLIF) on the other hand, gives more reliable information about the fuel-air mixing and the flame structure, advantages that qualify it as a suitable technique for the investigation of turbulent flames.

[1] PhD student, Email: amk74@cam.ac.uk
[2] Professor of Mechanical Engineering, Fellow AIAA, Email: apd1@cam.ac.uk
[3] Professor of Energy Technologies, Associate Fellow AIAA, Email: em257@eng.cam.ac.uk
[4] Lecturer in Systems Power and Energy, Email: Nader.Karimi@glasgow.ac.uk

Previous works from our group applied simultaneous OH* chemiluminescence and OH and CH_2O PLIF imaging, to provide a more accurate measurement of heat release rate in turbulent premixed flames[7-9]. As for most of such research until now, the imaging was done at a low sampling rate (5-10Hz). Recently-developed kHz-response PLIF systems, which have produced very interesting results on flame dynamics for ignition and extinction[10-12], have not been used yet widely for thermoacoustics studies.

One way of analysing such imaging data is through the application of the Proper Orthogonal Decomposition (POD) method, using the Sirovich's Method of Snapshots[13]. This method is frequently applied in order to reduce large datasets down to their most prominent spatial features (eigenmodes). The idea behind POD is to find a vector base for which the projection of the heat release fields (i.e. snapshots) on it maximizes the fluctuation energy for any subset of the base. POD has been used for self-excited flames by several groups in order to investigate flow-flame dynamics[14-18].

To improve our understanding of instability phenomena, an experimental investigation of lean swirling fully premixed turbulent self-excited flames undergoing thermoacoustic instabilities is presented. Flame dynamics are of particular interest, so high speed OH* chemiluminescence and OH PLIF techniques are used, in order to capture the motion of the flame and the dominant structures. The goal of the present work is to determine the effect of the burner geometry, equivalence ratio and flow velocity on the characteristic frequency of the burner and to reveal the dominant mechanisms. This work also focuses on the data post-processing aiming at extracting information about the dynamics that are not captured through the classical ensemble-averaging techniques.

II. Methods

A. Apparatus

For the purposes of the present study, a ca. 10kW atmospheric combustor was used (Figure 1). The combustor consists of two 300mm concentric circular ducts. The outer duct (inner diameter - i.d. = 35mm) houses two pressure taps (150mm axial distance), where pressure transducers were flush mounted with the duct internal wall, for acoustic pressure measurements. Care was taken to avoid cavity effects in the pressure measurement ports. Since pressure measurements were done upstream of the flame there was no need for cooling. At the exit of the inner duct (i.d. = 6mm) a conical bluff body of diameter 25mm was mounted for the stabilisation of the flame, giving a blockage ratio of 50%. Swirl was induced by a swirler with a vane angle of 60^o located 45mm upstream of the bluff body. The cold gases flowed through a 200mm long plenum chamber with an i.d. of 100mm. The plenum has divergent and convergent cross-sections at the inlet and the exit in order to avoid flow separation during expansion and contraction. Inside the plenum flow straighteners streamline the flow. The working section, which involves the reactive part of the flow, includes the region immediately downstream of the bluff-body. A quartz tube of internal diameter of 70 mm and length of 200 mm enclosed the working section and provided optical access to the flame. Self-excited acoustic instabilities were induced by extending the length of the tube downstream of the bluff body. For the results presented here the total length downstream of the bluff body was 210mm, 410mm or 510mm, with the former producing very low-amplitude oscillations and the latter producing very violent oscillations (discussed later).

Methane was used as a fuel and fully premixed flames were studied. In order to achieve the premixed condition at the bluff body, the air and methane are mixed far upstream the combustor (~2m) and flow through the plenum chamber. The flow conditions are characterized by the equivalence ratio, the combustor length, and the reactants bulk velocity at the inlet of the combustor (defined as the total flow rate divided by the open annular area between the bluff body and the outer duct).

B. Instrumentation

Two pressure transducers (Kulite XCS093, maximum pressure of 5 psi) were used to measure the pressure oscillations inside the upstream duct. Visualisation of the flame dynamics was accomplished by OH* chemiluminescence, and separately by OH PLIF measurements. As far as the former technique is concerned, a high speed Photron SA. 1.1 camera at 5 kHz was used for 1 s. This was done within the pressure measurement period. Measurements started at least 30 s after ignition, however in the course of the experiments this delay was extended to 1 minute or 90 s for different cases. As for the OH PLIF measurements, the same high speed camera was coupled with a LaVision IRO high-speed two-stage intensifier having a spectral range of 190–800 nm and fitted with a Cerco 2178 UV lens 100F/2.8 and OH filter. Details of both systems can be found in Ref. 11.

C. Data Post-Processing

The images were analysed using an in-house developed MATLAB code, based on the principles of Proper Orthogonal Decomposition[19]. The POD code, applied to a sequence of n temporally resolved heat release-field measurements, computes a set of n spatial eigenmodes $M_j(x,y)$ and projects the snapshots on each eigenmode to calculate the associated temporal coefficients $a_j(t)$. The calculated eigenvalues (λ_j), which represent the contribution of the modes to the overall kinetic energy of the flow, are sorted in decreasing order and thus the first modes represent the most energetic unsteady structures of the flow. The reconstruction of the snapshots using only the most energetic modes contributes to the understanding of the dominant mechanisms of the system. Since the results of the POD analysis for this dataset begin to converge after 500 snapshots, the POD method was applied to 1000 snapshots in order to achieve a good statistical representation. The acquired frames were 1024x1024 pixels but to reduce the computational cost they were cropped to the region of interest, which varied for different conditions. The time-average heat release field was subtracted from the data before the POD analysis in order to decompose only the fluctuating component.

Apart from the POD method, the post-processing analysis consisted of the application of the Fast Fourier Transform (FFT) to the pressure and to the spatially-integrated OH* intensity data in order to identify any periodic phenomena. The pressure spectrum acquired is indicative of the acoustic oscillation, whereas the integrated OH* intensity spectrum is proportional to the heat release perturbation. Spectra of the POD coefficients $a_j(t)$ were also calculated, enabled by the high-frequency sampling rate of the present OH* and OH PLIF systems.

III. Results and Discussion

A. General observations

Time series of OH* chemiluminescence images for the experimental condition φ=0.77 and L_{duct}=510mm are shown in Figure 2. The flame is anchored at the bluff body corner, with some evidence of flame movement into the outer recirculation zone associated with the sudden expansion from the inlet duct to the combustor section. There is evidence of a moving vortical structure in the axial direction, emanating from the interaction of the inlet flow and the bluff body. This interaction causes a flow separation that proceeds downstream. In order to further investigate this, the OH PLIF technique was used to visualize better the flame location. In

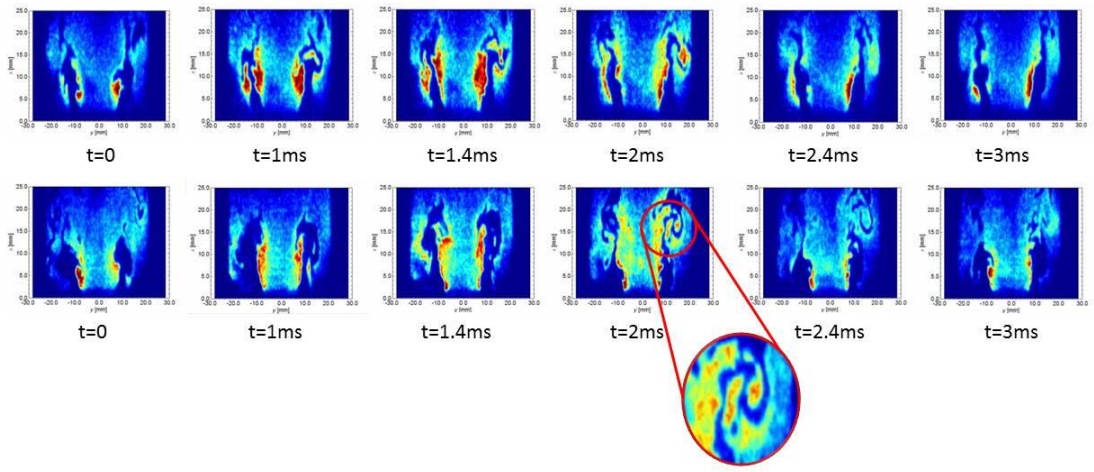

Figure 3~~Figure 3~~ snapshots from two conditions with the same equivalence ratio (φ=0.77) and different duct lengths (L_{duct}=410mm – top row, L_{duct}=510mm – bottom row) are compared.

The instant denoted as t=0 was arbitrarily chosen to be 2ms prior to the peak of the vortex formation for all conditions. From the observation of the timeframes sequence of the OH PLIF images for L_{duct}=510mm, it is evident that the vortex structure is very pronounced. In addition, in the case of L_{duct}=510mm at t=2ms, two sites of local flame annihilation are noted. This phenomenon occurs as the inner and outer flame fronts are brought together and it ultimately leads to an overall decrease in flame surface area and hence local heat release rate, as it has been reported before in externally forced flames[7, 9]. In these works, the magnitude of flame annihilation was found to be dependent on the amplitude of the induced forcing. In contrast, in the L_{duct}=410mm case, the vortical structures are not fully formed and the heat release appears to be more concentrated in the region above the bluff body. Comparing flames from the same duct length condition but of different equivalence ratios (Figure 4), it is found that the equivalence

ratio has an impact on the morphology of the flame roll-up. At low φ, roll-up is incomplete, while at higher φ the diameter of the flame roll-up around the vortex core is found to be decreased. This is in agreement with previous results[20].

In order to study the periodicity of the vortex in more detail and the effect of the equivalence ratio and of the duct length on its oscillation frequency, different operating conditions are examined. It was found that depending on the equivalence ratio, the pressure and heat release spectra can exhibit multiple peaks with significantly different frequencies, single peaks or not very clear peak structures. For example, the pressure spectrum of the flame with φ=0.77, U=10m/s and L_{duct}=510mm exhibits pressure fluctuations at 372 (f_1) and 263Hz (f_2), whereas the heat release spectrum exhibits heat release fluctuations at the same frequencies and at 109Hz (f_1-f_2), which is the linear combination of the other frequencies (Figure 5). This is due to the non-linear interactions of the two modes of oscillations. Operation at lower φ results in a single peak, which appears at the same frequency in both spectra. In addition, for some other conditions no definite peak structures are found. Also, it was observed that for a given operating condition the amplitude of the disturbance remains constant, whereas as the equivalence ratio increases the instability amplitude increases, since more energy is added to the system. Similar behaviour has been reported in Ref. 21.

The length of the duct has a distinct effect on the number and amplitude of fluctuations. Figure 5 presents the pressure and integrated OH* intensity spectra respectively for 3 different duct lengths. In the case of 210mm both spectra show low amplitudes and appear noisy with no distinct peak structures. At 410mm two noisy peaks around 395 and 265 Hz of higher amplitude are observed, while at 510mm distinct and high amplitude peaks are seen in the two spectra.

B. POD analysis

Having described the parameters that affect the flame-vortex interaction using conventional methods, a deeper investigation of the phenomenon is attempted by using the Proper Orthogonal Decomposition method. In fact, information about both the spatial structure and the periodicity of the vortex is acquired from the shape of the POD modes and the PSD of the POD time coefficients respectively.

Figure 6 (a) and (b) shows POD modes and their respective PSD for the 210mm duct length. In this case, no strong self-excited oscillations are identified in the PSD, denoting a thermo-acoustically stable flame, while the POD modes indicate that the flame had no strong features. Figure 6 (c) and (d) shows data for the 510mm duct length. In this case, the PSD shows the strong self-excited oscillations of the flame, and the multi-frequency components observed correspond to the dominant frequencies and to their linear combinations. The POD modes reveal a strong axial motion of the flame with little radial dependence. As the mode index increases the wavelength of this motion decreases. From the above, it can be deduced that the duct length appears to act as a resonating volume, which is transmitted to the flame and alters its structure. Also, modes 1 and 2 constitute a pair and have similar POD energy values, as it will be discussed shortly. In this study, it was found that the higher the equivalence ratio and the longer the duct length the stronger the self-excited oscillations were. For the majority of the cases exhibiting strong self-excited oscillations the mode shapes appeared to be in pairs and they usually had similar energy values.

Figure 7 shows the cumulative energy spectrum of the OH* chemiluminescence and OH PLIF data for different duct lengths. For the OH* chemiluminescence data, it is evident that up to mode 150, for a given mode number the longer the duct, the higher the cumulative energy is. This energy difference is much greater in the first few modes, the energy contribution of which is significantly larger than that of the successive modes. The first 200 modes capture 90.5%, 89% and 95.5% of the total energy for a dataset of 1000 images for 210, 410 and 510mm respectively. For the PLIF data, the cumulative energy contained in the first 200 modes was found to be 89% for L_{duct}=410mm and 88% for L_{duct}=510mm, which was similar to the POD energy of the OH* chemiluminescence data. However, the first few modes in the OH* chemiluminescence data contain significantly greater energy than those of the PLIF data. For example, for the condition L_{duct}=510mm the energy contained in the first two modes of the OH* chemiluminescence data is 63.5%, while that for the PLIF data is 11.5%. This is consistent with relevant findings in Ref. 22.

Figure 8 presents the relative energy content of each of the first 10 POD modes for L_{duct} =210mm (a) and L_{duct}=510mm (b). Both flames had the same equivalence ratio (φ=0.77). Modes 1 and 2 are the most energetic ones containing 3.8% and 3.2% respectively for 210mm and 34.1% and 29.8% respectively for 510mm. So, in the case of 510mm the total energy content of the first 2 modes is 9 times higher than that of the 210mm case. This is attributed to the fact that the energy is concentrated in a dominant structure, which is shown in the case of an axial moving vortex for the 510mm duct length, while there is a lack of such a structure in the 210mm case. Another striking feature is that the energy contained in mode 3 is constant (2.8%) for the case of 210mm and 510mm. This indicates that the dominant oscillating mechanism is captured by the first two modes. Also, it is worth noting that in the case

of 510mm, the modes appear to be in pairs of similar energy contents (1-2, 3-4, 5-6 and so forth). This observation, which has been reported before[23-25], constitutes a characteristic of single-frequency oscillations and has been attributed to vortex advection.

Having presented the different aspects of the POD analysis individually, graphs of the predominant oscillation frequency from the POD time coefficients, pressure and integrated OH* intensity spectra as well as of the pressure RMS values with respect to the parameters that influence them the most are presented and discussed collectively. The purpose of this analysis is to examine the interaction between the heat release and the acoustics.

Figure 9 shows the dominant frequency captured in the aforementioned spectra with respect to the equivalence ratio for different duct lengths. As shown in Figure 9 (a) the predominant oscillation frequency as obtained from the PSD of the POD time coefficients increases with φ in a range between 310 and 380 Hz. This might be attributed to the increase in laminar flame speed with the equivalence ratio. Figure 9 (b) and (c) show that the flame appears to be stable in the case of 210mm, as the lack of acoustic resonance manifests itself in a stable heat release. The matching of the pressure, heat release and PSD of POD time coefficients spectrum, which is in essence a representation of the heat release spectrum, denotes a strong interaction between the pressure and the heat release fluctuation. From Figure 9 (d), which plots the RMS of the pressure fluctuation with respect to φ, a maximum is observed at φ=0.77 for L_{duct}=510mm. This corresponds to a self-excited oscillation of 370Hz and its RMS value is approximately 60% greater than that at φ=0.7. At this point, taking into consideration that a cold flow velocity experiment using loudspeakers to induce a pressure fluctuation in the burner suggests that the burner exhibits a natural frequency at approximately 370Hz, it is possible that the aforementioned RMS peak value is amplified due to the resonance of the burner. As for L_{duct}=210mm, the RMS values are grouped into two clusters and they seem to be independent of φ.

In the same figure, the effect of cold flow velocity can also be observed. Figure 9 (a) shows that the dominant oscillation frequency, as obtained from the PSD of the POD time coefficients, increases with the cold flow velocity at the bluff body in a range between 310 and 370 Hz. Figure 9 (d) shows that for the case of U=10m/s, a maximum of the RMS amplitude of the acoustic pressure, with peak amplitude of 40 Pa occurring at φ=0.77, which might correspond to the resonant frequency of the burner as mentioned previously. For U=14m/s the RMS amplitude of the pressure is greater than that for U=10m/s between φ=0.70 and φ=0.74. This is probably due to the fact that at higher flame speed the heat release oscillations induce greater pressure fluctuations in the flow field. Also, for a given velocity, the RMS amplitude of the pressure increases with the the duct length. This was expected from the previous deduction that the longer duct length is linked to stronger self-excited oscillations and stronger patterns of the POD mode shapes.

The simultaneous examination of the banded shape of the low-order POD modes and the PSD of the corresponding coefficients allows the estimation of the convection speed of the vertical structure. This was determined by measuring the characteristic heat release wavelength (calculated from the most energetic POD modes) multiplied by the dominant frequency of the system as evaluated by the PSD of the same mode's POD time coefficient. In the literature the convection speed can be used to describe the spatial structure of the flow and is determined by either the frequency-wavenumber spectrum or by its Fourier transformation, which gives the space-time correlation function[26]. Figure 10 (a) shows a positive correlation between bulk velocity and convection speed. The effect of equivalence ratio however, is more complex and as such no unifying trend can be described. This is due to the fact that as it was presented in Figure 9 (a), the dominant frequency increases with φ, however the wavelength was found to be negatively correlated with the equivalence ratio. From Figure 10 (b) it can be deduced that for φ=0.70-0.87 and for U=10, 12, 14m/s the Convection Speed/Bulk Velocity=1.4-1.66. It is worth noting that the convection speed was found to be the same for the first four POD modes. In fact, both the wavelength of the dominant flow structure and the dominant frequency of these modes had the same values.

IV. Conclusion

In the present article we report our findings from the experimental investigation of lean, fully premixed, turbulent, self-excited flames undergoing thermoacoustic instabilities. Post-processing of the images acquired from OH* chemiluminescence and OH PLIF techniques was conducted using POD and FFT methods.

It was found that the duct acts as a resonating volume, which is transmitted to the flame and alters its structure. Similarly, equivalence ratio has an impact on the morphology of the flame roll-up. Subsequent POD analysis of the images revealed that the energy is concentrated in a dominant structure, which is shown in the case of an axial moving vortex. It was also observed that the higher the equivalence ratio and the longer the duct length the stronger the self-excited oscillations were. For the majority of the cases exhibiting strong self-excited oscillations the mode shapes appeared to be in pairs and they usually had similar energy values. The correspondence of the spectra of the

pressure, heat release and of the POD time coefficients denotes a strong interaction between the pressure and the heat release fluctuations. Post-processing of the image datasets from the two techniques revealed that, for a given number of modes, OH* chemilluminescence captures a higher percentage of the overall energy of the flame than OH PLIF does. Moreover, examination of the PSD of the POD time coefficients, pressure and heat release spectra revealed a distinct effect on the number of observed peaks and their corresponding frequencies. The dominant frequencies were also found to increase with cold flow velocity. The POD mode shapes and the corresponding coefficients spectral features allowed a determination of the convection speed. It was found that convection speed was positively correlated with bulk velocity, however the effect of equivalence ratio was more complex. This is due to the fact that, the dominant frequency increases with φ, however the wavelength was found to be negatively correlated with the equivalence ratio. Finally, the ratio of convection speed over bulk velocity was found to be in the fairly narrow range of 1.4-1.66.

Acknowledgments

This work was supported by European project IMPACT AE FP7-265586.

References

[1]McManus, K. R., Poinsot, T. and Candel, S. M., "A Review of Active Control of Combustion Instabilities". *Progress in Energy and Combustion Science*, Vol. 19, No. 1, 1993, pp. 1-29.

[2]Lee, J. G. and Santavicca, D.A., "Experimental Diagnostics for the Study of Combustion Instabilities in Lean Premixed Combustors". *Journal of Propulsion and Power*, Vol. 19, No. 5, 2003, pp. 735-750.

[3]Sadanandan, R., Stöhr, M. and Meier, W., "Flowfield-Flame Structure Interactions in an Oscillating Swirl Flame". *Combustion, Explosion and Shock Waves*, Vol. 45, No. 5, 2009, pp. 518-529.

[4]Kim, K. T. and Hochgreb, S., "The Nonlinear Heat Release Response of Stratified Lean-Premixed Flames to Acoustic Velocity Oscillations". *Combustion and Flame*, Vol. 158, No. 12, 2011, pp. 2482–2499.

[5]Steinberg, A. M., Boxx, I., Stöhr, M., Carter, C. D. and Meier, W., "Flow–Flame Interactions Causing Acoustically Coupled Heat Release Fluctuations in a Thermo-Acoustically Unstable Gas Turbine Model Combustor". *Combustion and Flame*, Vol. 157, No. 12, 2010, pp. 2250–2266.

[6]Worth, N. A. and Dawson, J.R., "Modal Dynamics of Self-Excited Azimuthal Instabilities in an Annular Combustion Chamber". *Combustion and Flame*, Vol. 160, No. 11, 2013, pp. 2476–2489.

[7]Balachandran, R., Ayoola, B. O., Kaminski, C. F., Dowling, A. P. and Mastorakos, E., "Experimental Investigation of the Nonlinear Response of Turbulent Premixed Flames to Imposed Inlet Velocity Oscillations". *Combustion and Flame*, Vol. 143, No. 1-2, 2005, pp. 37–55.

[8]Ayoola, B. O., Balachandran, R., Frank, J. H., Mastorakos, E. and Kaminski, C. F., "Spatially Resolved Heat Release Rate Measurements in Turbulent Premixed Flames". *Combustion and Flame*, Vol. 144, No. 1-2, 2006, pp. 1–16.

[9]Balachandran, R., Dowling, A. P. and Mastorakos, E., "Non-Linear Response of Turbulent Premixed Flames to Imposed Inlet Velocity Oscillations of Two Frequencies". *Flow Turbulence and Combustion*, Vol. 80, No. 4, 2008, pp. 455–487.

[10]Letty, C., Mastorakos, E., Masri, A. R., Juddoo, M. and O'Loughlin, W., "Structure of Igniting Ethanol and n-Heptane Spray Flames With and Without Swirl". *Experimental Thermal and Fluid Science*, Vol. 43, 2012, pp. 47-54.

[11]Kariuki, J., Dawson, J. and Mastorakos, E., "Measurements in Turbulent Premixed Bluff Body Flames Close to Blow-Off". *Combustion and Flame*, Vol. 159, No. 8, 2012, pp. 2589-2607.

[12]Cavaliere, D. E., Kariuki, J. and Mastorakos, E., "A Comparison of the Blow-Off Behaviour of Swirl-Stabilized Premixed, Non-Premixed and Spray Flames". *Flow Turbulence and Combustion*, Vol. 91, No. 2, 2013, pp. 347-372.

[13]Sirovich, L. and Kirby, M., "An Eigenfunction Approach to Large Scale Transitional Structures in Jet Flow". *Physics of fluids. A, Fluid dynamics*, Vol. 2, No. 2, 1990, pp. 127-136.

[14]Steinberg, A. M., Boxx, I., Stöhr, M., Meier, W., "Effects of Flow Structure Dynamics on Thermoacoustic Instabilities in Swirl-Stabilized Combustion". *AIAA Journal*, Vol. 50, No. 4, 2012, pp. 952-967.

[15]Iudiciani, P. and Duwig, C., "Large Eddy Simulation of the Sensitivity of Vortex Breakdown and Flame Stabilisation to Axial Forcing". *Flow, Turbulence and Combustion*, Vol. 86, No. 3-4, 2011, pp. 639–666.

[16]Moeck, J. P., Bourgouin, J.-F., Durox, D., Schuller, T. and Candel, S., "Nonlinear Interaction Between a Precessing Vortex Core and Acoustic Oscillations in a Turbulent Swirling Flame". *Combustion and Flame*, Vol. 159, No. 8, 2012, pp. 2650–2668.

[17]Stöhr, M., Boxx, I., Carter, C. D. and Meier W., "Experimental Study of Vortex-Flame Interaction in a Gas Turbine Model Combustor". *Combustion and Flame*, Vol. 159, No. 8, 2012, pp. 2636–2649.

[18]Boxx, I., Arndt, C. M., Carter, C. D. and Meier, W., "High-Speed Laser Diagnostics for the Study of Flame Dynamics in a Lean Premixed Gas Turbine Model Combustor". *Experiments in Fluids*, Vol. 52, No. 3, 2012, pp. 555–567.

[19]Ayache, S. and Mastorakos, E., "Investigation of the "TECFLAM" Non-Premixed Flame Using Large Eddy Simulation and Proper Orthogonal Decomposition". *Flow Turbulence and Combustion*, Vol. 90, No. 2, 2013, pp. 219–241.

[20]Renard, P.-H., Rolon, J., Thévenin, D. and Candel, S., "Investigations of Heat Release, Extinction, and Time Evolution of the Flame Surface, for a Nonpremixed Flame Interacting with a Vortex". *Combustion and Flame*, Vol. 117, No. 1-2, 1999, pp. 189–205.

[21]Muruganandam, T. M., Kim, B.-H., Morrell, M. R., Nori, V., Patel, M., Romig, B. W. and Seitzman, J. M., "Optical Equivalence Ratio Sensors for Gas Turbine Combustors". *Proceedings of the Combustion Institute*, Vol. 30, No. 1, 2005, pp. 1601–1609.

[22]Lombardi, S., Yuan, R., Continillo, G. and Mastorakos, E., "Proper Orthogonal Decomposition Analysis of an n-decane Swirling Spray Flame at Extinction". Submitted for publication.

[23]Bizon, K., Continillo, G., Russo, L. and Smuła, J., "On POD Reduced Models of Tubular Reactor with Periodic Regimes". *Computers and Chemical Engineering*, Vol. 32, No. 6, 2008, pp. 1305–1315.

[24]Ilak, M. and Rowley, C. W., "Modeling of Transitional Channel Flow Using Balanced Proper Orthogonal Decomposition". *Physics of Fluids*, Vol. 20, No. 3, 2008, pp. 034103.

[25]Rehimi, F., Aloui, F., Nasrallah S. B., Doubliez, L. and Legrand, J., "Experimental Investigation of a Confined Flow Downstream of a Circular Cylinder Centred Between Two Parallel Walls". *Journal of Fluids and Structures*, Vol. 24, No. 6, 2008, pp. 855–882.

[26]Del Álamo, J. C. and Jiménez, J., "Estimation of Turbulent Convection Velocities and Corrections to Taylor's Approximation". *Journal of Fluid Mechanics*, Vol. 640, 2009, pp. 5–26.

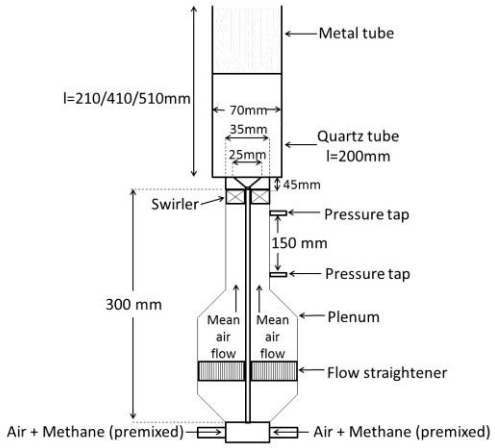

Figure 1. Schematic of the burner.

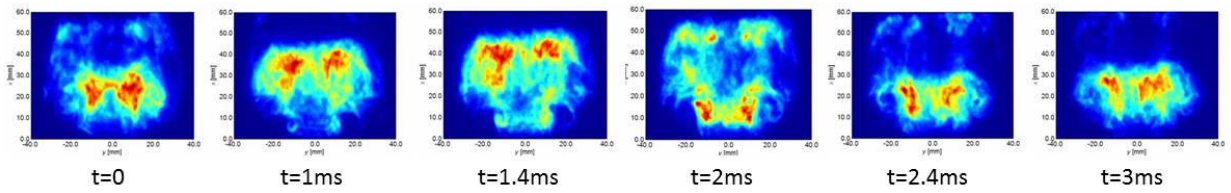

Figure 2 OH* chemiluminescence images at φ=0.77 and L_{duct}=510mm.

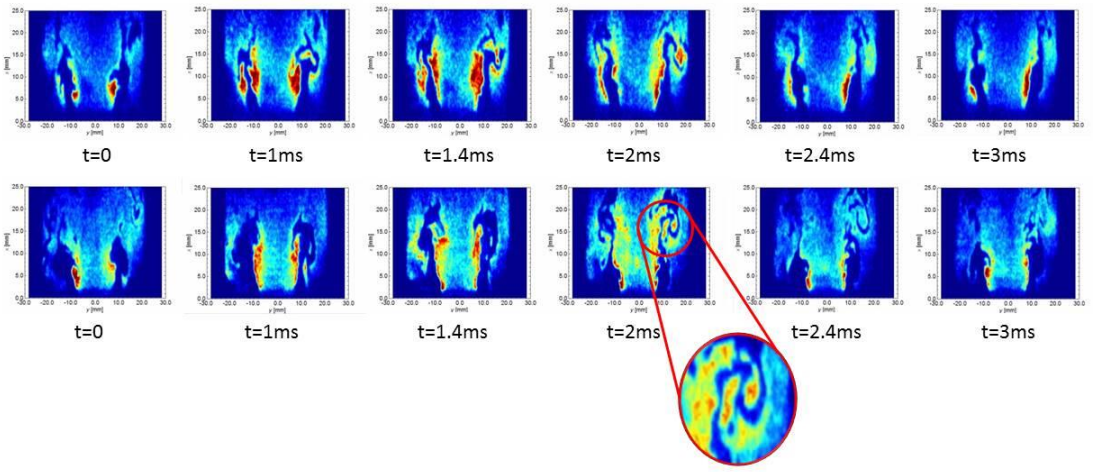

Figure 3 OH PLIF images at φ=0.77. Top row: L_{duct}=410mm, bottom row: L_{duct}=510mm. The detail from the condition L_{duct}=510mm at t=2ms, shows the area where local flame annihilation was found.

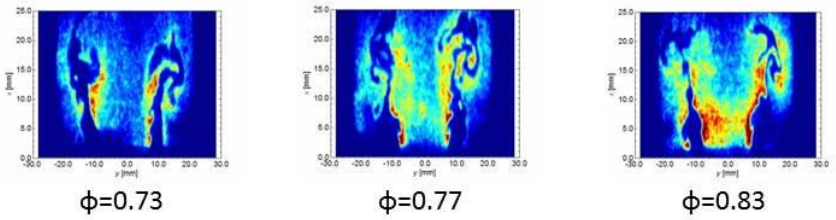

Figure 4 OH PLIF images at the time of maximum flame curvature from a burner equipped with a 510mm duct, operating at φ=0.73 (left),φ=0.77 (middle) and φ=0.83 (right).

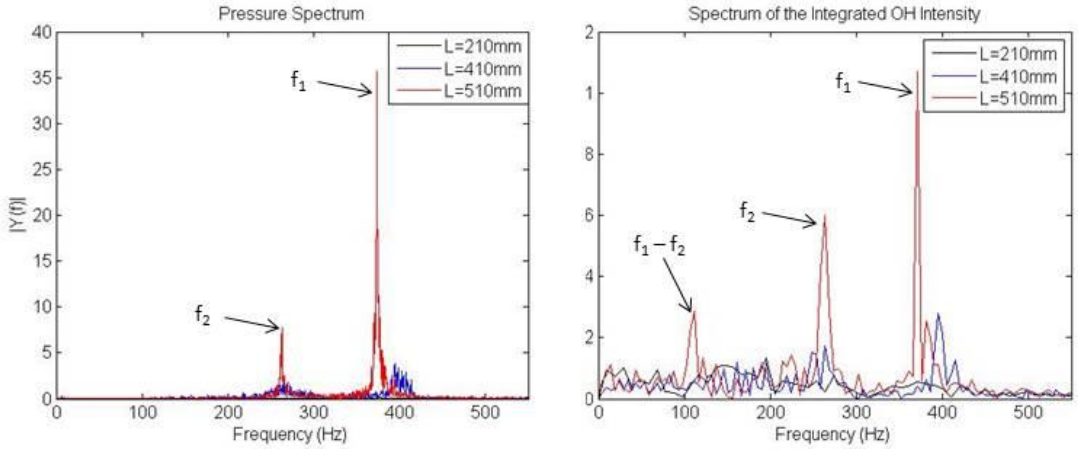

Figure 5 Pressure spectrum (a) and spectrum of integrated OH* intensity (b) for the different duct lengths. In all conditions φ=0.77 and U=10m/s.

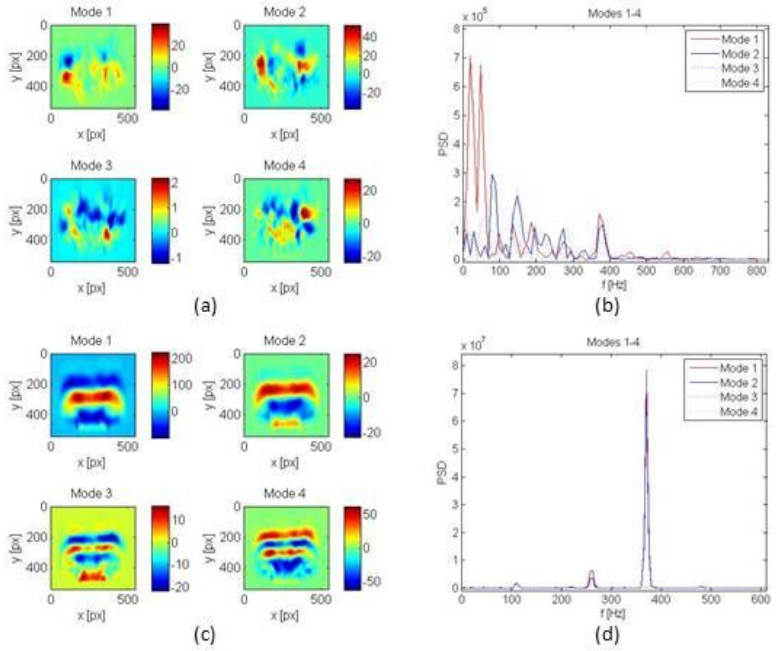

Figure 6 POD modes and their respective PSD for the condition φ=0.77, U=10m/s and L_{duct}=210mm (a and b) and L_{duct}=510mm (c and d).

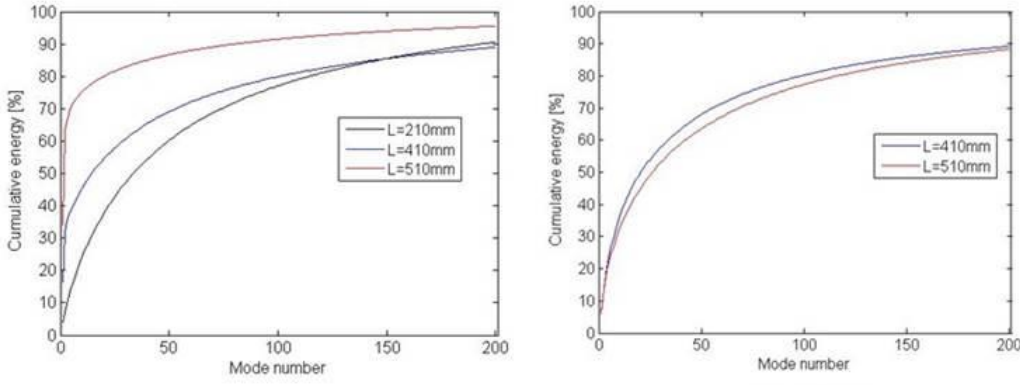

Figure 7 Cumulative energy spectrum of the POD modes from the OH* chemiluminescence (left) and OH PLIF (right) data for the 3 different duct lengths. For all conditions: U=10m/s and φ=0.77.

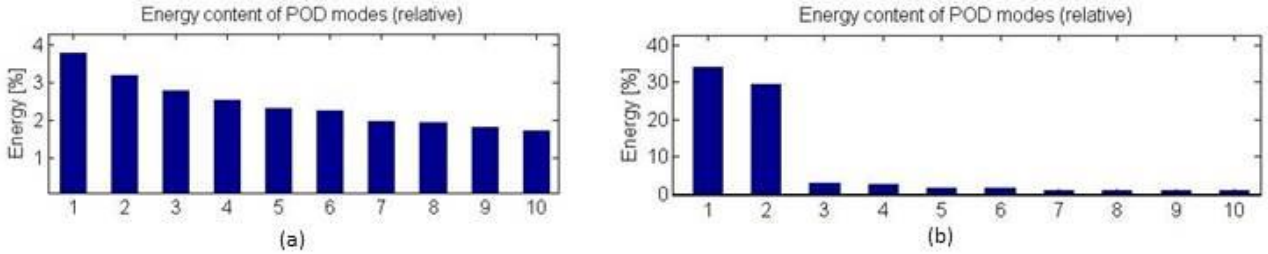

Figure 8 Energy content (%) of the first 10 modes captured from OH* chemiluminescence. The flame had φ=0.77 in a combustor with (a) L_{duct}=210mm and (b) L_{duct}=510mm.

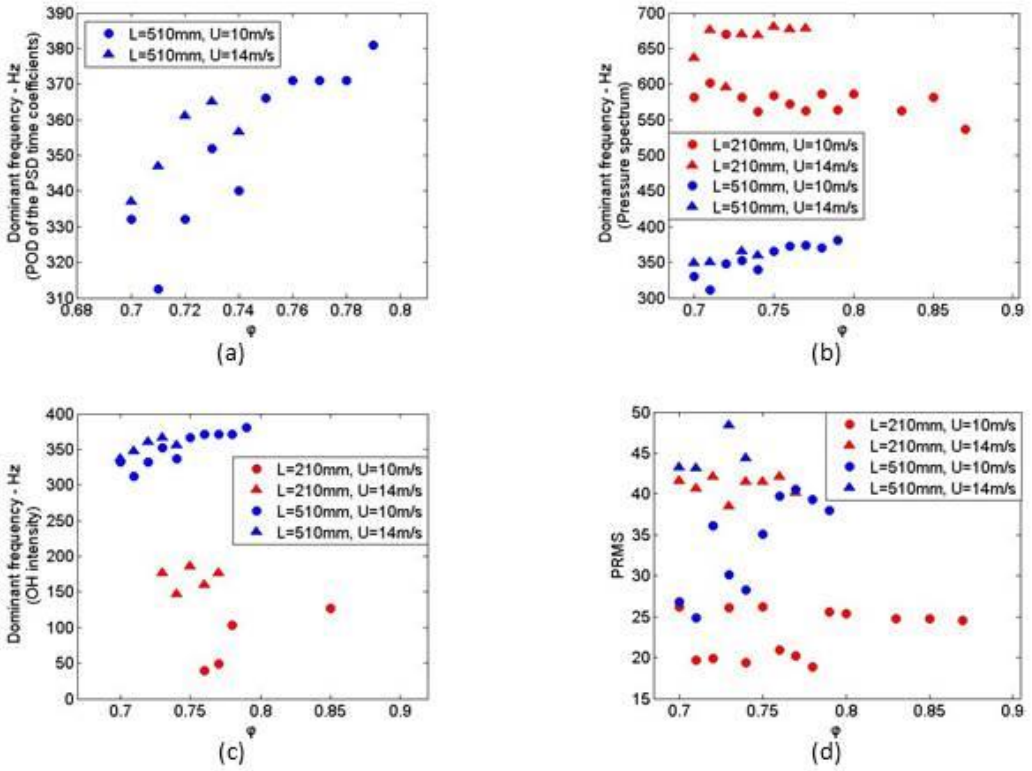

Figure 9 Results of the FFT analysis for all the experimental conditions visualized by OH* chemiluminescence. (a) Dominant frequency POD of the PSD time coefficients, (b) Dominant frequency pressure spectrum, (c) Dominant frequency spatially-integrated OH* intensity, (d) pressure root mean square, all as a function of equivalence ratio for duct lengths L_{duct}=210mm and L_{duct}=510mm and for U=10m/s and U=14m/s.

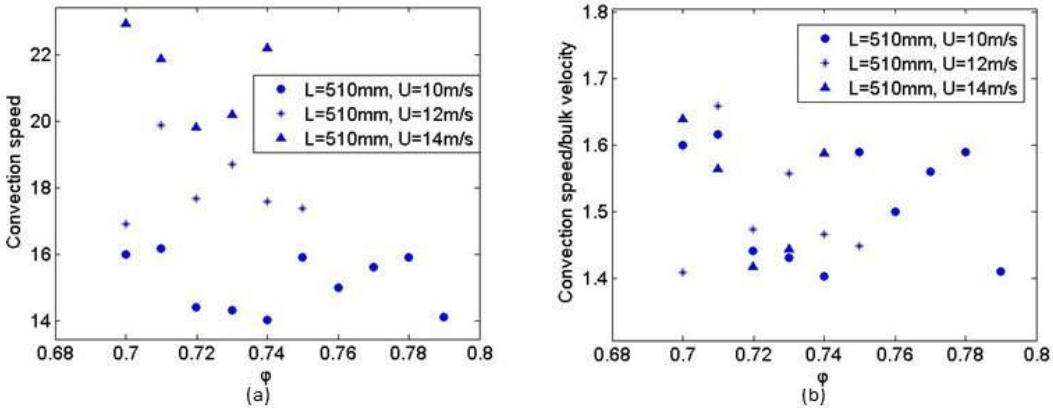

Figure 10 Convection speed as a function of φ for L_{duct}=510mm and different values of bulk velocity (a). The same data divided by bulk velocity (b).